Biointerface Research in Applied Chemistry
Open-Access Journal (ISSN: 2069-5837)

Article
Volume 13, Issue 6, 2023, 535
https://doi.org/10.33263/BRIAC136.535

Natural Illitic Clay as an Eco-Friendly Adsorbent for Removal of Cu (II) Ions from Aqueous Solution: Experimental Study, Data Modeling, and Monte Carlo Simulation

Otheman Amrhar [1,*], Mohamed Mobarak [2], Avni Berisha [3,4], Mohamed S. ElYoubi [5], Hakima Nassali [6]

[1] Department of Chemistry, Faculty of Sciences, Ibn Tofail University, Kenitra, Morocco; otheman.amrhar@gmail.com (O.A.);
[2] Physics Department, Faculty of Science, Beni–Suef University, Beni–Suef, Egypt; Saidan2011@yahoo.com (M.M.);
[3] Department of Chemistry, Faculty of Natural and Mathematics Science, University of Prishtina, Prishtina, Kosovo
[4] Materials Science - Nanochemistry Research Group, NanoAlb, Unit of Albanian Nanoscience and Nanotechnology, Tirana, Albania ; avni.berisha@uni-pr.edu (A.B.);
[5] Department of Chemistry, Faculty of Sciences, Ibn Tofail University, Kenitra, Morocco; mselyoubi@yahoo.fr (M.S.E.);
[6] Department of Chemistry, Faculty of Sciences, Ibn Tofail University, Kenitra, Morocco; hnassali@yahoo.fr (H.N.);
* Correspondence: otheman.amrhar@gmail.com (O.A.);

Scopus Author ID 57003587700
Received: 5.10.2022; Accepted: 19.11.2022; Published: 6.02.2023

Abstract: Adsorption using clays is a preferred technique for removing heavy metals from aqueous solutions. Understanding adsorption at the molecular level is important for a good optimization of the removal process. In the present work, the experimental and theoretical studies of Cu(II) ions adsorption on Natural Illitic Clay (NIC) were realized. An experimental investigation was carried out to highlight the effect of some experimental parameters on the adsorption efficiency. Then, modeling of the adsorption data and Monte Carlo simulation (MCS) were performed to explain the adsorption process at the molecular level. The experimental results showed that equilibrium was reached after 120 min and that the basic pH of the solution was favorable for good adsorption. Interpretation of the equilibrium isotherms showed that increasing the temperature from 25 to 45 °C increased the adsorbed amount from 3.6582 to 3.8041 $mg.g^{-1}$, and promoted the aggregation of copper ions, which caused a hindrance effect by preventing their access to the adsorption sites on the surface of the NIC. Modeling of the adsorption kinetics indicated that external and intra-particle diffusion steps occurred simultaneously and contributed to the rate-controlling of the adsorption process. Adsorption energy values determined by computational simulation showed a considerable affinity of $[Cu(H_2O)_4]^{2+}$ towards the deprotonated (010) surface of the illite mineral compared to protonated (010) surface.

Keywords: adsorption; Cu(II) ions; natural illitic clay; statistical physics approach; adsorption kinetics; Monte Carlo simulation.

1. Introduction

The presence of heavy metals in industrial effluents is an environmental issue for living beings and human health [1]. Copper (II), classified as a priority pollutant [2], is one of the most common heavy metals in effluents from industrial activities. According to EPA, drinking water's maximum acceptable concentration of copper (II) is 1.3 $mg.L^{-1}$ [3]. High copper (II)

doses can cause serious toxicological problems for human health [4]. It is, therefore important to treat industrial effluents before they are discharged into waterways. Various treatment techniques have been developed and applied to reduce high concentrations of heavy metals. However, the adsorption technique remains the best and most preferred technique for wastewater treatment [5]. In addition, equilibrium isotherms and kinetic data obtained from adsorption experiments can be mathematically modeled to understand the adsorption process better. Equilibrium isotherms modeling involves using models that can be classified into two categories. i.e., classical isotherm models and statistical physic models. Classical isotherm models are established for some adsorption systems, and their assumptions are not appropriate for all other systems [6]. As the classical models are not related to the parameters that can influence the removal of the adsorbate, a better interpretation of the equilibrium isotherm cannot be obtained [7,8]. To overcome these limitations, the statistical physics approach is introduced in order to establish models that can reflect the state of the adsorption systems [9]. On the other hand, the adsorbate/adsorbent interface can be studied by exploiting kinetic data through the application of kinetic models. These models can be classified into two categories. i.e., Adsorption Diffusion Models (ADMs) and Adsorption Reaction Models (ARMs) [10]. ADMs represent the external diffusion and intra-particle diffusion steps, while the ARMs characterize the surface reaction stage.

Various materials are used as adsorbents in wastewater treatment [11–15]. The use of natural clay materials in wastewater treatments has received particular attention due to their many advantages [16–18]. Among the clay materials, illite clay is used as a natural adsorbent for wastewater treatment [19]. It is a 2:1 phyllosilicate with a very limited tendency to swell because the interlayers are linked together by non-solvated potassium ions (K^+) [3]. Generally, 2:1 clay minerals present the permanent charge (responsible for the cation exchange capacity (C.E.C)) located in the interlayer space and on the external basal surface of the clay mineral, and the variable charge is located on the surface of the edge [20]. Since the K^+ cations in the interlayer space of the illite clay are not exchangeable, the permanent charge's contribution to the cationic ions' adsorption process remains limited.

On the other hand, the surface of the edges can play a determining role in the adsorption of heavy metal ions. Indeed, this surface is characterized by the presence of AlO-, SiO-, and AlOH- groups resulting from the broken (010) surface of the clay mineral. These groups, which represent the seat of the variable charge, can be protonated/deprotonated depending on the pH of the adsorption medium [21,22]. As a result, they can repel/attract heavy metal cations and contribute to the de-pollution of wastewater during the adsorption process.

Recently, molecular simulation has become a powerful and indispensable tool in studying various chemical phenomena at the molecular level [23–25], particularly in the study of the different interactions between pollutants and clays [26,27]. For example, Lammers *et al*. [28] studied the adsorption of cesium (Cs) on the edge, basal plane, and interlayer surfaces of illite nanoparticles by molecular simulation and found that the edge and interlayers surface has a higher affinity for Cs than the basal planes. Qiu *et al*. [29] investigated the effect of protonation and deprotonation of kaolinite surfaces on the adsorption of rare earth elements. They showed that the adsorption energy of deprotonation is much higher than that of protonation for both (010) and (001) surfaces studied.

Numerous studies have been carried out to valorize illite clay as a natural adsorbent in the treatment of wastewater loaded with heavy metal ions [30–32]. However, to the best of our knowledge, there are not enough articles that model the adsorption isotherms of heavy metal

ions on illite clay according to the statistical physics approach to obtain a thorough understanding of the adsorption of heavy metals on solid surfaces. So, the present study aims to: i) Use the Natural Illitic Clay (NIC) as the natural and eco-friendly adsorbent in the removal of Cu(II) cation as a model ion from the aqueous solution and to highlight the effect of some experimental parameters on the adsorption efficiency. ii) Examine the equilibrium isotherms obtained and estimate the kinetic parameters using various mathematical models better to understand the adsorption process at the molecular level. iii) Carry out a molecular simulation of the adsorption of hydrated copper ion on the (010) surface of illite clay according to Monte Carlo Simulation (MCS) to illustrate the impact of protonation and deprotonation of this surface on the adsorption efficiency.

2. Materials and Methods

2.1. Natural illitic clay.

The raw Natural Illitic Clay (NIC) used in this study was extracted from a quarry located in the region of Khemisset (northwest of Morocco). After washing with distilled water, it was dried in an oven at 110°C for 2 hours to remove residual water, then crushed, sieved, and stored in a dry bottle for future experiments [33]. The mineralogical composition of the NIC, determined using the XPERT-PRO diffractometer, indicated that it is composed of illite and quartz minerals, with a trace of kaolinite [19]. The wavelength dispersion spectrometer - Type Axios- was used to determine the composition of the oxide in the NIC. This composition revealed the presence of silica (61.7%) and alumina (24.6%) as major oxides, as well as traces of potassium (3.28%), iron (2.62%), magnesium (1.55%), calcium (0.558%), sodium (0.513%) and titanium(0.575%) oxides [19]. The Metson method was used to determine the cation exchange capacity (C.E.C) [34]. The value obtained (22.54 meq.100g^{-1}), which is within the range indicated in the bibliography [35], can be explained by the fact that the illite mineral is a non-ionic clay which is characterized by the absence of cation exchange proprieties in the interlayer space, although it can present isomorphic substitutions in its structure [36], it can exchange cations located on the surface of the edges with other cations in the medium [37]. The specific surface was measured according to the method of Santamarina *et al*. [38] and showed a value equal to 18.2 m^2.g^{-1}. The elemental composition of NIC was determined by atomic absorption spectroscopy and showed the significant presence of Si, Al, and O elements. The pH corresponding to the point zero charges of the surface of the NIC particles (pH_{PZC}) was determined according to the literature [19]. All the physicochemical proprieties obtained are listed in Table 1.

Table 1. Physicochemical properties and elemental composition of NIC.

Specific surface (m^2.g^{-1})		18.2
C.E.C (meq.100g^{-1})		22.54
Point of zero charge (pH_{PZC})		8.2*
Elemental composition (%)	**Si**	34.4
	Al	25.8
	O	24.4
	K	9.9
	Fe	3.1
	Mg	2.5

*Reported by Amrhar *et al.* [19]

2.2. Adsorption experiments.

A stock solution was prepared by dissolving $CuSO_4,5H_2O$ in distilled water. The required initial concentrations were obtained by dilution of the stock solution. The adsorption experiments were carried out using the batch technique to determine the influence of certain physicochemical parameters on the adsorption of copper ions by NIC. 0.4 g of NIC was added to 20 mL of the Cu(II) ion solution with the required initial concentration. After stirring under the conditions to be studied, and filtration, the residual concentration was measured using the Varian SpectrAA 220 Atomic Absorption Spectrometer. The adsorbed amount of Cu(II) ions was calculated using the following expression [7]:

$$Q_e = \frac{(C_0 - C_e)}{m} V \quad (1)$$

With C_0 ($mg.L^{-1}$) and C_e ($mg.L^{-1}$) are the initial and equilibrium concentration of Cu(II) ions in the solution, respectively, V (L) is the volume of the solution, and m (g) is the mass use of NIC.

The adsorption experiments were carried out to determine the equilibrium time with an initial copper concentration of 50 $mg.L^{-1}$ and a pH of 6. The contact time was varied from 0 to 300 min. The adsorbed amount of Cu(II) ions at an instant t was calculated using the following relation:

$$Q_t = \frac{(C_0 - C_t)}{m} V \quad (2)$$

With C_t ($mg.L^{-1}$) is the equilibrium concentration of Cu(II) ions in solution at an instant t.

2.3. Equilibrium isotherm modeling.

The equilibrium isotherm represents the variation of the adsorbed quantity of metal ions as a function of the equilibrium concentration. Its representation makes it possible to determine the maximum adsorption capacity of the adsorbent when the adsorption process reaches equilibrium. Giles *et al*. [39] proposed a classification of equilibrium isotherms according to their shape and initial slope. Limousin *et al*. [40] reviewed this classification, distinguishing four types of isotherms: The S isotherm (Sigmoid), the L isotherm (Langmuir), the H isotherm (high affinity), and the C isotherm (constant partition). On the other hand, modeling the equilibrium isotherm is essential for studying the interactions between the pollutant to be removed and the adsorbent used during the adsorption. Several classical isotherm models have been proposed and developed in the literature to model the equilibrium isotherms mathematically and to study the possible interactions between the adsorbate and the adsorbent. Recently, the statistical physics approach has been introduced, and mathematical models have been developed to improve the understanding of the adsorption process at the molecular level [9]. In the present study, four classical isotherm models and five statistical physics models were used to model the obtained equilibrium isotherms which are presented in Table 2. The valid mathematical model for interpreting the obtained equilibrium isotherms was selected based on the values of the coefficient of determination R^2 and the Chi-square according to the nonlinear regression method.

$$\chi^2 = \sum_{i=1}^{n} \frac{\left(Q_{e\,exp} - Q_{e\,cal}\right)_i^2}{Q_{e\,cal}}$$

2.4. Adsorption kinetics modeling.

Adsorption kinetics discusses the variation of the adsorbed amount of a species over time. It provides more information about the adsorption mechanism and explains how the adsorbate moves from the liquid phase to the solid phase [41]. Generally, the adsorption process consists of four steps: 1) The transport of the adsorbate from the solution to the external film surrounding the solid particle (to be neglected if the adsorption system is in agitation).2) The passage of the adsorbate through the external film to the surface of the solid particle (this step is called "external diffusion"). 3) The diffusion of the adsorbate into the pores of the solid particle (so-called "intra-particle diffusion"). 4) The adsorption on sites located on the inner surface of the solid particle (known as "adsorption reaction") [7]. Habitually, the second and third steps are limiting steps in the adsorption kinetics [42,43], but in some cases, combining these two steps controls the adsorption process [44]. In this work, the experimental data obtained from the adsorption kinetics were analyzed using the models presented in Table 3.

Table 2. Equilibrium isotherm models used in the present study.
$C_{1/2}$ (mg.L^{-1}) and C_e (mg.L^{-1}) are the concentration at half-saturation, and the equilibrium concentration, respectively; N_m (mg.g^{-1}) is the density of receptor sites on clay; C^a and C^b are the concentrations at half-saturation of the first and the second receptor site respectively; C_1 and C_2 represent the concentrations at half-saturation associated with the first and the second layers, respectively; N_l represents the average number of layers. ***** For more details, the reader is invited to consult the reference [51].

	Model	Expression	Ref.
Classical isotherm models	Freundlich	$Q_e = K_F C_e^{1/n}$ (3)	[45]
	Langmuir	$Q_e = \frac{Q_{max} K_L C_e}{1+K_L C_e}$ (4)	[46]
	D-R	$Q_e = Q_{max} \exp\left(-B_D\left[RT \ln\left(1+1/C_e\right)\right]^2\right)$ (5)	[47]
	Temkin	$Q_e = \frac{RT}{b} \mathrm{Ln}(K_t C_e)$ (6)	[48]
Statistical physics models*	Monolayer model with one energy of adsorption	$Q = \frac{n.N_m}{1+\left(\frac{C_{1/2}}{C_e}\right)^n}$ (7)	[9,49]
	Monolayer model with two energies of adsorption	$Q = \frac{n_1.N_{m1}}{1+\left(\frac{C^a}{C_e}\right)^{n_1}} + \frac{n_2.N_{m2}}{1+\left(\frac{C^b}{C_e}\right)^{n_2}}$ (8)	[49,50]
	Double-layer model with one energy of adsorption	$Q = n \times N_m \frac{\left(\frac{C}{C_{1/2}}\right)^n + 2\times\left(\frac{C}{C_{1/2}}\right)^{2n}}{1+\left(\frac{C}{C_{1/2}}\right)^n + \left(\frac{C}{C_{1/2}}\right)^{2n}}$ (9)	[49,50]
	Double-layer model with two energies of adsorption	$Q = n \times N_m \frac{\left(\frac{C}{C_1}\right)^n + 2\times\left(\frac{C}{C_2}\right)^{2n}}{1+\left(\frac{C}{C_1}\right)^n + \left(\frac{C}{C_2}\right)^{2n}}$ (10)	[9,49]

	Model	Expression	Ref.
	Finite multilayer model	$\frac{\left(\frac{C}{C_i}\right)^{N_c}\left[1+(N_c+1)\left(\frac{C}{C_i}\right)^{nN_c}+N_c\left(\frac{C}{C_i}\right)^{n(N_c+1)}\right]}{(Q-nN_c)\frac{\left(\frac{C}{C_i}\right)^{N_c}}{\left[1+\left(\frac{C}{C_i}\right)^{n}\right]\left[1+\left(\frac{C}{C_i}\right)^{n}+\left(\frac{C}{C_i}\right)^{2n}+\left(\frac{C}{C_i}\right)^{3n}+\left(\frac{C}{C_i}\right)^{nN_c}\right]}}$ (11)	[49,50]

Table 3. Kinetic models used in the present study.

	Kinetic model	Expression	Ref.
Adsorption Diffusion Models (ADMs)	Furusawa and Smith model	$\ln\left[\frac{C_t}{C_0}-\frac{A}{m_S K_L}\right]=-\frac{K_f S t}{A}+\ln A$ (12) With: $A=\frac{m_S K_L}{1+m_S K_L}$ (13)	[52]
	Boyd model	$Ln\left[1-\frac{q_t}{q_e}\right]=-Rt$ (14) With: $R=\frac{3D_e}{r_0 \Delta r_0 k}$ (15)	[53]
	Weber and Morris model	$Q_t=k_{int}t^{1/2}+C'$ (16)	[54]
	Boyd model for intra-particle	$F>0.85 \Rightarrow Bt= -0,4977 - \ln(1-F)$ (17) $F<0.85 \Rightarrow Bt= 2\pi - \frac{\pi^2 F}{3} - 2\pi\left(1-\frac{\pi F}{3}\right)^{1/2}$ (18) With: $D_i=\frac{r_0^{\,2} B}{\pi^2}$ (19)	[53]
Adsorption Reaction Models (ARMs)	Pseudo-first order model	$Ln(Q_e - Q_t)= Ln\, Q_e - k_1 t$ (20)	[55]
	Pseudo-second order model	$\frac{t}{Q_t}=\frac{1}{k_2 Q_e^{\,2}}+\frac{t}{Q_e}$ (21)	[56,57]

S(cm^{-1}) is the specific surface of the interface solid/liquid; K_L ($L.mg^{-1}$) is the constant of Langmuir; K_f ($cm.min^{-1}$) is the coefficient of the external mass transfer; m_s=m/v ($g.cm^{-3}$) is the mass of the adsorbent by the unit of volume; r_0 (cm) is the ray of an adsorbent particle; Δr_0 (cm) is the thickness of liquid film (Δr_0=r'-r_0); K_{int} ($mg.g^{-1}.min^{-1/2}$)is the rate constant of intra-particle diffusion model; C' ($mg.g^{-1}$) is the constant depends on the thickness of the boundary layer; D_e is the constant of diffusion in the liquid film; k is the constant of effectiveness of the adsorbate distribution; F is the report of the adsorbed quantity q_t at the moment t and that adsorbed q_e at equilibrium; B (min^{-1}) is the rate constant; k_1 (min^{-1}) is the rate constant of pseudo-first-order adsorption; k_2 ($g.mg^{-1}.min^{-1}$) is the rate constant of pseudo-second-order adsorption.

2.5. Monte Carlo simulation method.

To study the impact of protonation and deprotonation of the edges surface of the illite mineral on copper ion adsorption, Monte Carlo simulation (MCS) was performed in an aqueous medium. First, the unit cell of the illite mineral (a = 5.20210 Å, b = 8.97970Å, c = 10.2260Å, α = 90.00°, β = 101.57°, γ = 90.00°) was constructed according to crystallographic data available in the literature [58] using the Crystal builder module implemented in the Materials Studio2017 software [59]. To simulate the edge of the illite mineral, the unit cell created was cleaved at the (010) plane. Under periodic boundary conditions, the unit cell was duplicated 4 times in the x-direction to obtain the super-cell. To model the protonated (010) surface of illite (noted "illite (010)proto"), the –Si-O-, -Al-O-, and -Al-OH groups on the (010) surface were saturated with H atoms. The deprotonated (010) surface of illite (noted "illite (010)deproto") was obtained by removing all hydrogen atoms on the (010) surface. On the other hand, it is known that the Cu^{2+} ion has several coordination configurations in water to form $[Cu(H_2O)_n]^{2+}$ complexes (n=1-6) [60]. According to Burda *et al*. [61], the Cu(II) ion prefers to coordinate with four water molecules in the first hydration shell. So, in this study, the hydration of the Cu(II) ion was performed by constructing the $[Cu(H_2O)_4]^{2+}$ complex. Then the optimization of its structure was executed using the $Dmol^3$ module according to the Generalized Gradient Approximation (GGA) with the Perdew-Burke-Enzerhof (PBE) functional [62] (Figure S1, Supplementary Information).

The Adsorption Locator module in Materials Studio software was used to determine the best adsorption configurations and to calculate the adsorption energy of $[Cu(H_2O)_4]^{2+}$ on illite(010)proto and illite (010)deproto. For this, the $[Cu(H_2O)_4]^{2+}$/illite(010)deproto and $[Cu(H_2O)_4]^{2+}$/illite(010)proto structures were geometrically optimized according to the Smart algorithm [63] using the Compass II force field [64,65]. The Ewald summation method was used to treat electrostatic interactions with an accuracy of 1×10^{-3} kcal.mol^{-1}, while Van der Waals interactions were examined using the atom-based summation with 12.5 Å as the cut-off distance (with a spline width of 1 Å) [66]. 3 cycles of simulated annealing were applied with 15000 steps for each cycle, and the annealing temperature was set between 10^5 and 10^2 K [67]. From the obtained adsorption configurations, the affinity of $[Cu(H_2O)_4]^{2+}$ toward the edge surface of the illite mineral (i.e., the illite (010) surface) was evaluated after the calculation of the adsorption energy E_{ads} using the following relation [27]:

$$E_{ads} = E_{total} - (E_{surface+solution} + E_{[Cu(H_2O)_4]^{2+}}) \quad (22)$$

Where E_{total} represent the total energy of the $[Cu(H_2O)_4]^{2+}$/illite(010) system. $E_{surface+solution}$ characterise the energy of the illite (010) surface and the solution without $[Cu(H_2O)_4]^{2+}$. $E_{[Cu(H2O)4]^{2+}}$ is the energy of $[Cu(H_2O)_4]^{2+}$. A high absolute value of E_{ads} is an indication of a high affinity between $[Cu(H_2O)_4]^{2+}$ and the illite (010) surface [68]. To calculate the adsorption energy E_{ads}, the total energy E_{total} of the optimized structure (i.e., $[Cu(H_2O)_4]^{2+}$/illite(010)) was first calculated. Then, the adsorbent phase was deleted from the optimized structure in order to calculate the energy of $[Cu(H_2O)_4]^{2+}$ ($E_{[Cu(H2O)4]^{2+}}$). Similarly, $[Cu(H_2O)_4]^{2+}$ was deleted from the optimized structure, and the surface energy of the illite mineral with solution $E_{surface+solution}$ was calculated [27,66].

3. Results and Discussion

3.1. Effect of contact time.

Figure 1 illustrates the effect of contact time on the adsorption of Cu(II) ions onto the NIC. The adsorption of Cu(II) ions occurred in two phases, with equilibrium reached after 120 min. In the first phase, the adsorption rate of Cu(II) ions was higher due to the availability of adsorption sites on the NIC surface, which favors the attraction of copper ions and thus accelerates their adsorption. This first phase was followed by a slow phase indicating a decrease in the number of adsorption sites [19]. Thus, no significant increase in metal ion removal was detected during this second phase.

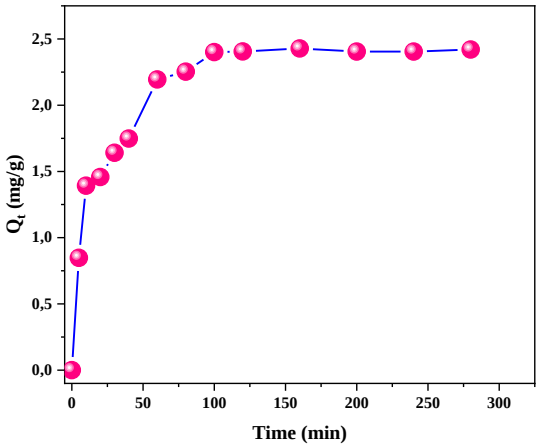

Figure 1. Effect of contact time on the adsorption of Cu(II) ions onto NIC (C_0=50 mg.L^{-1}, NIC mass=0.4g, T=25°C).

3.2. Effect of solution pH.

pH is one of the important parameters that can influence the adsorption behavior of heavy metals on suspended clay particles [69–71]. To study the effect of solution pH, experiments were carried out at room temperature with a Cu(II) ions concentration of 70 mg.L^{-1}.

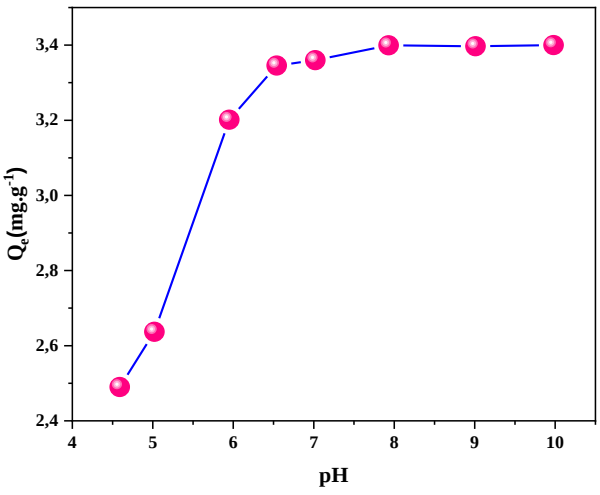

Figure 2 Effect of solution pH on the adsorption of Cu(II) ions onto NIC (C_0=70 mg.L^{-1}, NIC mass =0.4g, T=25°C).

According to Figure 2, the amount of copper ions adsorbed depends on the pH value. Indeed, the Q_e increased from 2.49 to 3.4 $mg.g^{-1}$ when the pH increased from 4.6 to 10. In the acidic medium, the H^+ present in the solution competes with the copper ions to access the adsorption surface, making the charge of the edges of the clay positive (protonation of the surface of the edge), which hinders the adsorption of Cu(II) ions. With increasing pH, the concentration of H^+ in the solution decreases, so the competition between H^+ and Cu(II) ions also decreases. As a result, deprotonation of the surface of the edge occurs, making the charge of this surface progressively negative. The adsorption of copper ions improves through the formation of inner-sphere complexes [72].

3.3. Effect of initial Cu(II) concentration.

The effect of initial concentration on the adsorption of Cu(II) ions onto NIC particles was studied using initial concentrations up to 150 $mg.L^{-1}$. From Figure 3, the amount of Cu(II) ions removed at equilibrium increases with the initial concentration, indicating that the removal of Cu(II) ions depends on their initial concentration. Increasing the initial concentration allows the development of driving forces that can minimize the resistance to the transfer of Cu(II) ions from the liquid to the solid phase and thus contribute to improving the adsorption efficiency [73]. At high initial concentrations, the adsorbed amount of Cu(II) ions reached a plateau, indicating a decrease in removal efficiency due to the saturation of the NIC particle surface. Similar results were reported for the adsorption of copper ions onto natural clays [74].

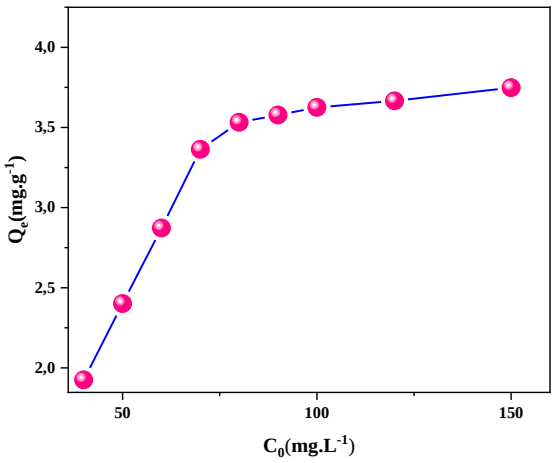

Figure 3. Effect of initial concentration on the adsorption of Cu(II) ions onto NIC (pH= 6, NIC mass =0.4g, T=25°C).

3.4. Equilibrium isotherms modeling and theoretical interpretation.

The variation of the adsorbed amount of Cu(II) ions as a function of the residual concentration at three temperatures (i.e., 25, 35, and 45°C) is shown in Figure 4. According to Gil's classification [39], these equilibrium isotherms display an L curve pattern, indicating a high affinity between the NIC particles and Cu(II) ions. At low concentrations, these isotherms have a convexity turned upwards due to the saturation of the surface of the NIC particles and a decrease in the number of adsorption sites as the adsorption process advances.

3.4.1. Modeling using classical isotherm models.

Generally, the equilibrium isotherm is examined by its parameters, whose values characterize the adsorbent's surface properties and the adsorbate's affinity towards the latter [75]. The isotherm parameters obtained by the nonlinear regression method after applying the classical isotherm models are presented in Table 4. The best R^2 values correspond to Langmuir and D-R models and are comparable. So, to determine the adequate model among these two models, the Chi-square χ^2 was used. As shown in Table 4, the D-R model is adequate to represent the equilibrium data with the lowest χ^2 values, indicating that the adsorption of Cu(II) ions takes place on both heterogeneous and homogeneous adsorption sites [49]. All values of adsorption energy calculated from the D-R model are lower than 8 $kJ.mol^{-1}$, indicating the physical nature of Cu(II) ions adsorption on the surface of NIC [76].

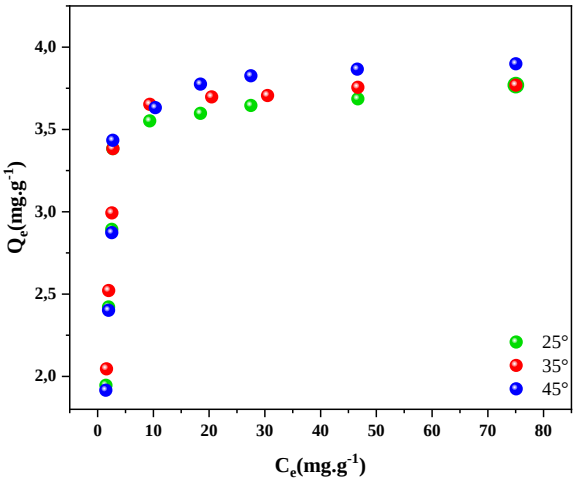

Figure 4. Equilibrium isotherms of Cu(II) ions adsorption onto NIC at different temperatures (NIC mass =0.4g)

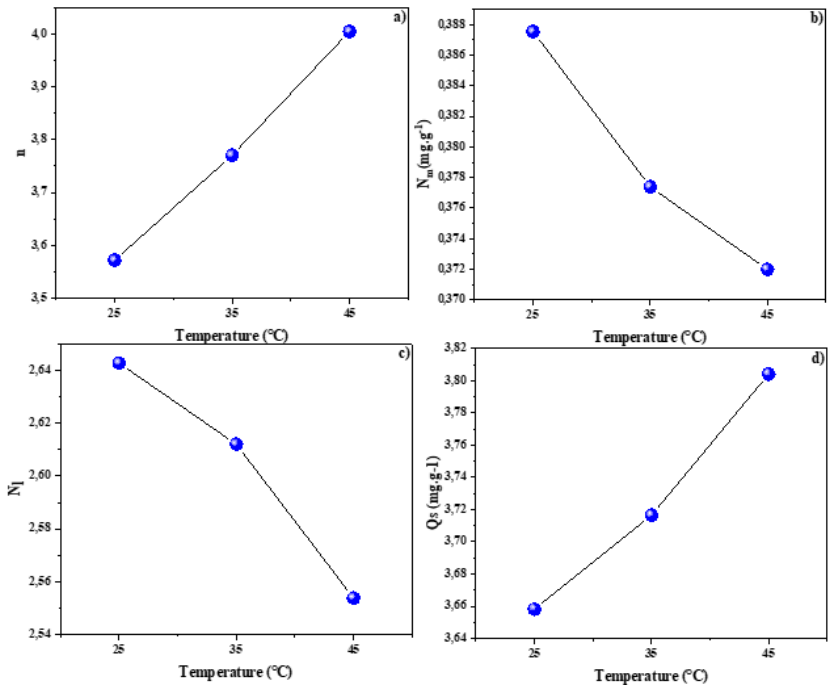

Figure 5. Variation of (**a)** n parameter values, (**b)** N_m parameter values, (**c)** N_l parameters values, (**d)** adsorbed quantity at saturation Q_{sat} as a function of temperature.

Table 4. Isotherm parameters after application of classical models.

	25°C	35°C	45°C
Freundlich			
K_F(L.g^{-1})	1.866	1.922	1.907
1/n	0.198	0.193	0.202
R^2	**0.777**	**0.775**	**0.798**
χ^2	**0.407**	**0.411**	**0.394**
Langmuir			
Q_{max}(mg.g^{-1})	3.858	3.904	4.006
K_L(L.mg^{-1})	0.948	0.969	0.885
R^2	**0.958**	**0.953**	**0.943**
χ^2	**0.077**	**0.086**	**0.111**
D-R			
Q_{max}(mg.g^{-1})	3.848	3.888	3.968
B_D	0.415	0.404	0.422
E(Kj.mol^{-1})	1.098	1.112	1.088
R^2	**0.958**	**0.953**	**0.942**
χ^2	**0.071**	**0.079**	**0.104**
Temkin			
B	4.394	4.431	4.294
K_T(L.g^{-1})	27.326	30.994	28.379
R^2	**0.891**	**0.887**	**0.899**
χ^2	**0.199**	**0.206**	**0.197**

3.4.2. Modeling using statistical physics models

To improve the interpretation of the equilibrium isotherms and to describe the adsorption of Cu(II) ions at the molecular level, five statistical physics models mentioned above were applied according to the Levenberg-Marquardt iterating algorithm. The adequate model was selected on the basis of the values of the coefficient of determination R^2 and the chi-square χ^2. According to Table 5, the highest R^2 and the lowest χ^2 correspond to the finite multilayer model, indicating that this model is adequate to fit equilibrium isotherms of the studied adsorption system. The estimated values of the steric parameters (i.e., n, N_m, N_l, and Q_s) and energetic parameters ($-\varepsilon_1$ and $-\varepsilon_2$) corresponding to the finite multilayer model are summarized in Table 6.

Table 5. Values of the coefficient of determination R^2 and the chi-square χ^2.

	25°		35°		45°	
	R^2	**χ^2**	**R^2**	**χ^2**	**R^2**	**χ^2**
Monolayer model with one energy of adsorption	0.958	0.084	0.953	0.094	0.959	0.092
Monolayer model with two energies of adsorption	0.993	0.021	0.998	0.006	0.985	0.047
Double-layer model with one energy of adsorption	0.959	0.082	0.954	0.093	0.961	0.088
Double-layer model with two energies of adsorption	0.959	0.091	0.984	0.036	0.961	0.098
Finite multilayer model	**0.993**	**0.019**	**0.998**	**0.005**	**0.985**	**0.041**

Table 6. Estimated values of fitted parameters corresponding to the finite multilayer model.

Temperature	n	N_m(mg.g^{-1})	N_l	$-\varepsilon_1$(kJ.mol^{-1})	$-\varepsilon_2$(kJ.mol^{-1})	Q_{sat}(mg.g^{-1})
25°	3.57186	0.38755	2.64269	-36.109	-29.908	3.6582
35°	3.77024	0.37739	2.612	-37.466	-30.895	3.7165
45°	4.00431	0.37199	2.55383	-38.712	-31.73	3.8041

The n parameter gives an idea about the geometrical orientation of the Cu(II) ions adsorbed on the surface of NIC particles and their possible aggregation [77]. Indeed, if n<1, the Cu(II) ions are anchored horizontally, which means that the adsorption process is multi-anchorage. If n=1, the Cu(II) ions are arranged laterally, which indicates that the adsorption is a mono-adsorbate process, but if n>1, many Cu(II) ions anchor in a single adsorption site with the possibility of their aggregation, which reflects that the adsorption is a multi-adsorbate

process [78,79]. From Table 6, all n values are greater than 1 (3.57186<n<4.00431), reflecting a possible aggregation of copper ions in each adsorption site, and thus, the adsorption of Cu(II) ions on the surface of NIC particles is a multi-adsorbate process. Figure 5-a) shows the variation of n values with temperature. Increasing the temperature raises the values of n, which reflects a promotion of the aggregation reaction of copper ions at high temperatures and indicates the endothermic nature of this reaction [80]. This behavior can be explained by the fact that at high temperatures, the mobility of Cu(II) ions in solution becomes easy [9], which favors their displacement towards the adsorption sites and therefore promotes their aggregation [81].

The N_m parameter refers to the number of identical adsorption sites occupied by the adsorbate when the adsorption process reaches saturation [51,81]. As shown in Table 6 and Figure 5-b), increasing the temperature leads to a decrease in the value of N_m. This variation is opposite to that of the parameter n. Indeed, the increase in the degree of aggregation of Cu(II) ions with temperature caused a hindrance effect that prevents the access of ions to other adsorption sites. Consequently, the density of the adsorption site decreases [82].

Another important steric parameter is the N_l parameter. It represents the average number of adsorbate layers formed at equilibrium. From Table 6, the N_l value varies between 2.6427 and 2.5538, indicating that the adsorption of Cu(II) ions on the NIC particles occurred by forming more than two layers. The evolution of N_l as a function of temperature (Figure 5-c) has an opposite tendency to that of the n parameter. Indeed, the evolution of the parameter n with temperature indicates that the horizontal ionic interactions between copper ions on the surface of NIC particles (caused by the aggregation reaction) are favorable compared to the vertical ionic interactions, which makes the increase in the number of layers unfavorable with the increase in temperature [83].

The amount of Cu(II) ions adsorbed at saturation Q_{sat} is calculated by multiplying the other steric parameters (i.e., $Q_{sat}=n\times N_m\times N_l$). According to Figure 5-d), the temperature has a positive effect on the amount adsorbed at saturation. The increase in temperature improved the Q_{sat}, which reflects an endothermic character of the adsorption of Cu(II) ions on NIC particles. Since Q_{sat} is correlated with other steric parameters, its increase can be explained mathematically by the increase in the number of Cu(II) ions adsorbed by an adsorption site (increase in the value of the parameter n). Thus, the parameter n can be considered the parameter controlling the adsorption process of Cu(II) ions on the surface of NIC particles.

On the other hand, the comparison of the adsorption capacity obtained for the NIC with other studies reported in the literature is presented in Table 7. The NIC shows a similar adsorption capacity compared to other clay materials, making it possible to consider NIC as a potential material for treating wastewater containing Cu(II) ions.

Table 7. Comparison of the adsorption capacity of Cu(II) ions by some clay materials.

Clay material (origin)	Q_{max} (mg.g^{-1})	Ref.
Palygorskite (Clay Minerals Repository, Florida)	2.35 (at 25°C)	[84]
Natural Illitic Clay (Morocco)	3.6582 (at 25°C)	Present work
Kaolinite (Iran china Clay Industries Co.)	4.42 (at 20°C)	[85]
Montmorillonite (Aldrich Chemicals Co)	7.62 (at 25°C)	[86]
Sepiolite (Yazd (Iran))	8.68 (at 25°C)	[84]
Clinoptilolite (North Greece)	13.6 (at 25°C)	[87]
Goethite (India)	37.25 (at 30°C)	[88]

In order to examine the possible interactions that may occur during the adsorption of copper ions by the NIC, two adsorption energies were calculated according to the finite multilayer model [9]:

$$-\varepsilon_1 = RT\ln\left(\frac{C_S}{C_1}\right) \quad (23)$$

$$-\varepsilon_2 = RT\ln\left(\frac{C_S}{C_2}\right) \quad (24)$$

where ($-\varepsilon_1$) and ($-\varepsilon_2$) represents the interaction energies between Cu(II) ions and the surface of NIC particles and between Cu(II)-Cu(II) ions (vertical ionic interactions), respectively. C_1 and C_2 are related to the concentrations at half-saturation, and C_S is the solubility of copper in water. From Table 6, the absolute value of $-\varepsilon_1$ is greater than that of $-\varepsilon_2$ ($|-\varepsilon_1|>|-\varepsilon_2|$), indicating that the interactions between copper ions and adsorption sites on the NIC surface are more important than the vertical ionic interactions between copper ions. All the absolute values of the adsorption energies do not exceed 40 kJ.mol^{-1}, which indicates the physical nature of the adsorption of Cu(II) ions on the surface of NIC particles [77]. The absolute value of ($-\varepsilon_1$) and ($-\varepsilon_2$) increases with temperature, which confirms the endothermic character of the adsorption process.

3.5. Kinetics data analysis

The ADMs and ARMs models mentioned in Table 3 were used to model the kinetic data of Cu(II) ion adsorption on NIC particles and calculate the corresponding values. The obtained curves are presented in Figure 6.

The Furusawa and Smith and Boyd models were used to illustrating the importance of the external diffusion step in the adsorption of Cu(II) ions. As shown in Figure 6-a), the application of the Furusawa and Smith model to the kinetic data is not appropriate (R^2 = 0.7546). Application of the Boyd model to the experimental data shows a line that does not pass through the origin (Figure 6-b) [53], which means that external diffusion through the liquid film surrounding the NIC particles was not only the limiting step in the adsorption of Cu(II) ions.

The Weber and Morris model and Boy's model for intra-particle diffusion were applied to show the intra-particle diffusion step's contribution to the copper ions' adsorption process. The curve corresponding to the Weber and Morris model (Figure 6-c) is not straight over the time interval tested and can be divided into two linear regions reflecting two adsorption steps. The first line shows the fast adsorption step, which corresponds to a mass transfer of Cu(II) ions from the liquid phase to the external surface of the NIC particles (film diffusion step). The second line indicates the slow adsorption step with the diffusion of Cu(II) ions through the pores of the NIC particles (intra-particle diffusion step). The two lines do not pass through the origin, indicating that film diffusion and intra-particle diffusion occurred simultaneously [53,54]. It is important to note that the value of the rate constant corresponding to the intra-particle step K_2 (calculated from the slope of the second line) is lower than that of the external diffusion step K_1 (calculated from the slope of the first line) (K_2 = 0.0127 mg.g^{-1}.min$^{-½}$ < K_1=0.2624 mg.g^{-1}.min$^{-½}$). This can be explained by considering the thickness of the liquid film surrounding the NIC particles. Indeed, the value of the intercept C' (which represents the thickness of the liquid film) of the second line (C'_2= 2.2271 mg.g^{-1}) is higher than that of the first line (C'_1= 0.2232 mg.g^{-1}). This leads to an increase in the mass transfer resistance from the

liquid film to the internal pores of the NIC particles, and consequently, the rate constant decreases. On the other hand, the application of the Boyd model for intra-particle diffusion (Figure 6-d) shows that it does not pass through the origin, confirming that intra-particle diffusion was not the dominant step in controlling the rate of Cu(II) ions adsorbed onto the surface of the NIC particles. The application of these two intra-particle diffusion models confirmed that both external and intra-particle diffusion steps occurred simultaneously and contributed to the rate-controlling of the adsorption of copper ions onto the surface of NIC particles.

Figure 6-e-f) shows the plots of the pseudo-first-order model and the pseudo-second-order model corresponding to the adsorption of copper ions on NIC particles. The value of the coefficient of determination R^2 for the pseudo-second-order model is close to 1 ($R^2 > 0.99$) compared to that of the pseudo-first-order model. The value of the adsorbed amount of cooper ions calculated from the pseudo-second-order model ($Q_{e,cal}$ = 2.5157 mg.g^{-1}) is closer to that obtained experimentally ($Q_{e,exp}$ = 2.4201 mg.g^{-1}) (Table 8). These results indicate that the kinetic data of the adsorption of Cu(II) ions are perfectly fitted using the pseudo-second-order model.

Table 8. Parameters of surface reaction models for Cu(II) ions adsorption onto NIC.

	Pseudo-first order kinetic model			**Pseudo-second order kinetic model**		
$Q_{e,exp}$ (mg.g^{-1})	**K_1 (min^{-1})**	**$Q_{e,cal}$ (mg.g^{-1})**	**R^2**	**K_2 (g.mg^{-1}.min^{-1})**	**$Q_{e,cal}$ (mg.g^{-1})**	**R^2**
2,4201	0.0242	1.1845	0.8275	0.0418	2.5157	0.9975

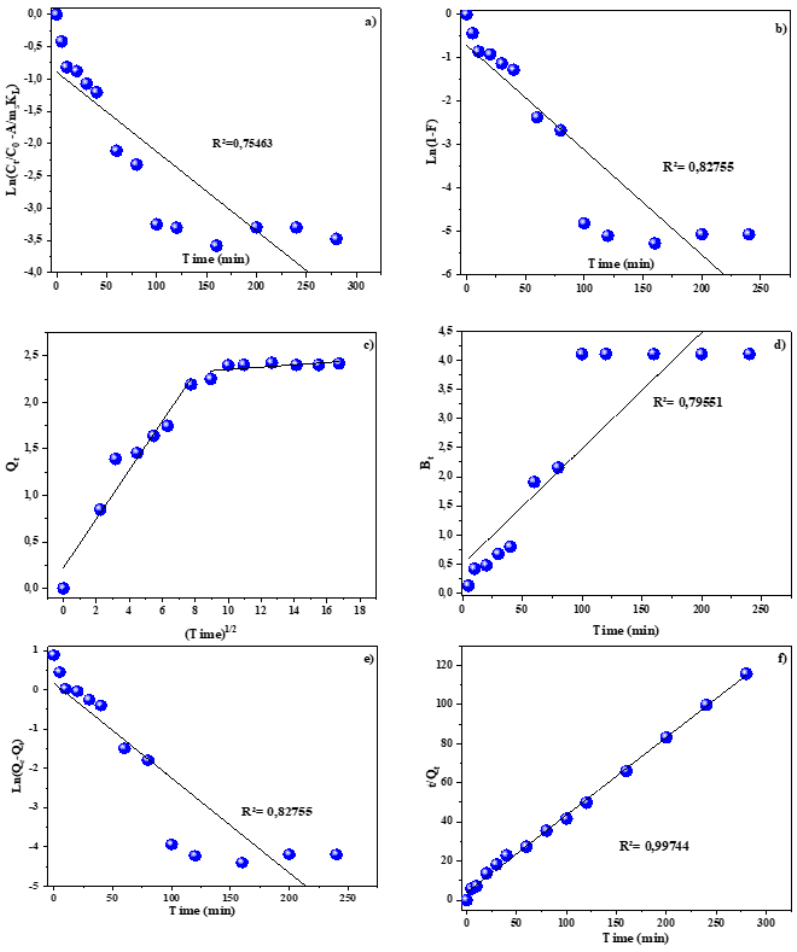

Figure 6. Application of (**a)** Furusawa and Smith model, (**b)** Boyd model, (**c)** Weber and Morris model, (**d)** Boyd model, (**e)** pseudo-first-order model, and (**f)** pseudo-second-order model on the kinetic data of Cu(II) ions adsorption onto NIC.

3.6. Monte Carlo simulation results

Monte Carlo simulation (MCS) was carried out to evaluate the influence of protonation and deprotonation of the illite (010) surface on the affinity of the latter towards $[Cu(H_2O)_4]^{2+}$. Firstly, the adsorption energy distribution of $[Cu(H_2O)_4]^{2+}$ on illite (010)deproto and illite (010)proto was calculated, and the results obtained are presented in Figure S2 (Supplementary Information). The adsorption energy values of $[Cu(H_2O)_4]^{2+}$ vary between -194.35 and -156.85 Kcal.mol^{-1} in the case of illite (010)proto, and between -326.1 and -167.3 Kcal.mol^{-1} in the case of illite (010)deproto, which indicates the high ability of $[Cu(H_2O)_4]^{2+}$ to be adsorbed on both illite (010)proto and illite (010)deproto surfaces [89].

Fluctuations in the interaction energies of $[Cu(H_2O)_4]^{2+}$ with illite (010)proto and illite (010)deproto are determined by optimizing the simulated systems (Figure S3, Supplementary Information) and the best adsorption configurations obtained are presented in Figure 7. It is clear that hydrated Cu^{2+} forms an inner-sphere complex with illite (010)deproto since the copper ion shows a tendency to interact with the deprotonated oxygen on the adsorption surface (dCu^{2+}-O=1.67Å). When Cu^{2+} approaches the protonated (010) surface, the hydrogens on the surface interact with the oxygen in the water ligands to facilitate the adsorption of copper ion and form an outer-sphere complex (dH_{177}-O_{182}=1.681Å; dH_{172}-O_{184}=2.219Å). On the other hand, the affinity of $[Cu(H_2O)_4]^{2+}$ towards the studied adsorption surfaces was evaluated by calculating the adsorption energy E_{ads}. The E_{ads} values show a considerable affinity between illite (010)deproto and $[Cu(H_2O)_4]^{2+}$ compared to that between illite (010)proto and $[Cu(H_2O)_4]^{2+}$ ($|E_{ads}|$(illite (010)deproto) = 1.188×10^3 Kcal.mol^{-1}> ($|E_{ads}|$(illite (010)proto) = 1.067×10^3 Kcal.mol^{-1}). These results indicate that the hydrated copper ion shows a good preference for interacting with the deprotonated (010) surface of illite compared to the protonated (010) surface, which is consistent with the results obtained from the pH effect experiments (section 3.2).

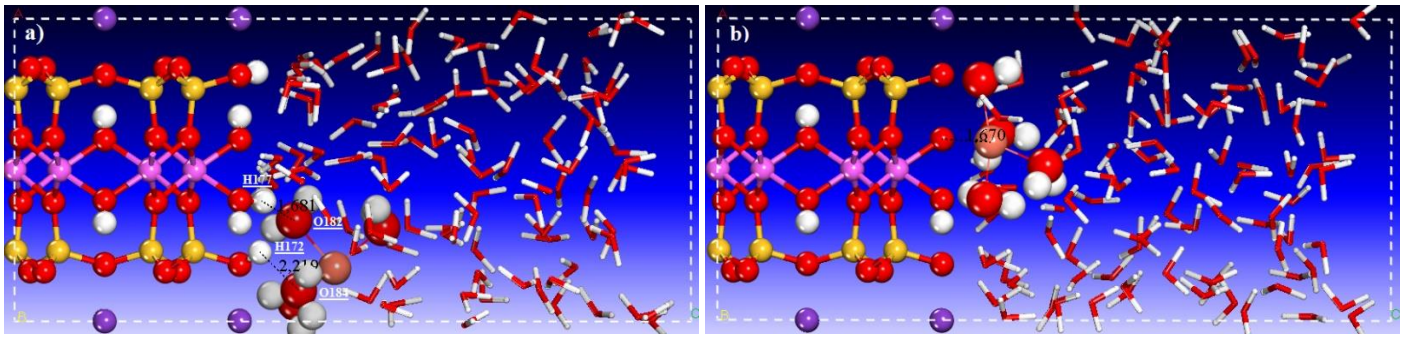

Figure 7. Best configurations of $[Cu(H_2O)_4]^{2+}$ adsorption onto a) illite (010)proto b) illite (010)deproto, according to Monte Carlo simulation.

4. Conclusions

In this work, the removal of Cu(II) ions from aqueous solution by adsorption on the natural illitic clay were investigated, and the adsorption process was interpreted at the molecular level by modeling the adsorption data and performing Monte Carlo simulation. The following conclusions could be drawn from this study:

The amount of adsorbed copper ions increases with the increasing pH of the solution as well as with increasing initial concentration.

Analysis of equilibrium isotherms indicates that the adsorption of Cu(II) ions occurred on homogeneous and heterogeneous adsorption sites with possible aggregation of the ions in each adsorption site. Consequently, a hindrance effect occurred and made the increase in the number of adsorbate layers unfavorable at high temperatures.

Analysis of the kinetic data shows that the external and intra-particle diffusion steps are the rate-limiting steps for the adsorption of copper ions onto NIC particles.

The best adsorption configuration and adsorption energy determined by Monte Carlo simulation show a high affinity between the hydrated copper ion and the deprotonated (010) surface of illite compared to the protonated (010) surface.

Funding

The present work did not receive any specific finance from funding establishments in the public, commercial, or not-for-profit sectors.

Acknowledgments

The authors of the present work thank the anonymous referees for their useful remarks and suggestions.

Conflict of interest

There is no conflict of interest in this work.

References

1. Chuah, T.G.; Jumasiah, A.; Azni, I.; Katayon, S.; Thomas Choong, S.Y. Rice Husk as a Potentially Low-Cost Biosorbent for Heavy Metal and Dye Removal: An Overview. *Desalination* **2005**, *175*, 305–316, https://doi.org/10.1016/j.desal.2004.10.014.
2. Environmental Protection Agency. Aquatic life ambient freshwater quality criteria -Copper-. *U.S. Environmental Protection - Agency Office of Water Office of Science and Technology Washington, DC* **2007**. https://www.epa.gov/sites/default/files/2019-02/documents/al-freshwater-copper-2007-revision.pdf.
3. Uddin, M.K. A Review on the Adsorption of Heavy Metals by Clay Minerals, with Special Focus on the Past Decade. *Chemical Engineering Journal* **2017**, *308*, 438–462, https://doi.org/10.1016/j.cej.2016.09.029.
4. Bouhamed, F.; Elouear, Z.; Bouzid, J. Adsorptive Removal of Copper(II) from Aqueous Solutions on Activated Carbon Prepared from Tunisian Date Stones: Equilibrium, Kinetics and Thermodynamics. *Journal of the Taiwan Institute of Chemical Engineers* **2012**, *43*, 741–749, https://doi.org/10.1016/j.jtice.2012.02.011.
5. Fu, F.; Wang, Q. Removal of Heavy Metal Ions from Wastewaters: A Review. *Journal of Environmental Management* **2011**, *92*, 407–418, https://doi.org/10.1016/j.jenvman.2010.11.011.
6. Al-Ghouti, M.A.; Da'ana, D.A. Guidelines for the Use and Interpretation of Adsorption Isotherm Models: A Review. *Journal of Hazardous Materials* **2020**, *393*, 122383, https://doi.org/10.1016/j.jhazmat.2020.122383.
7. Amrhar, O.; Berisha, A.; El Gana, L.; Nassali, H.; S. Elyoubi, M. Removal of Methylene Blue Dye by Adsorption onto Natural Muscovite Clay: Experimental, Theoretical and Computational Investigation. *International Journal of Environmental Analytical Chemistry* **2021**, 1–26, https://doi.org/10.1080/03067319.2021.1897119.
8. Sellaoui, L.; Guedidi, H.; Knani, S.; Reinert, L.; Duclaux, L.; Ben Lamine, A. Application of Statistical Physics Formalism to the Modeling of Adsorption Isotherms of Ibuprofen on Activated Carbon. *Fluid Phase Equilibria* **2015**, *387*, 103–110, https://doi.org/10.1016/j.fluid.2014.12.018.
9. Yazidi, A.; Sellaoui, L.; Dotto, G.L.; Bonilla-Petriciolet, A.; Fröhlich, A.C.; Lamine, A.B. Monolayer and Multilayer Adsorption of Pharmaceuticals on Activated Carbon: Application of Advanced Statistical Physics Models. *Journal of Molecular Liquids* **2019**, *283*, 276–286, https://doi.org/10.1016/j.molliq.2019.03.101.

10. Raji, F.; Pakizeh, M. Kinetic and Thermodynamic Studies of Hg(II) Adsorption onto MCM-41 Modified by ZnCl2. *Applied Surface Science* **2014**, *301*, 568–575, https://doi.org/10.1016/j.apsusc.2014.02.136.
11. Mohammadi, L.; Baniasadi, M.; Rahdar, A.; Kyzas, G.Z. Removal of Acid Dye from Aqueous Solutions with Adsorption onto Modified Wheat Bran – Modeling with Artificial Neural Networks. *Biointerface Res Appl Chem* **2021**, *11*, 14044–14056, https://doi.org/10.33263/BRIAC116.1404414056.
12. Refaat El Awady, F.; Ali Abbas, M.; Abdelghany, A.M.; El-Amir, Y.A. Silver Modified Hydrophytes for Heavy Metal Removal from Different Water Resources. *Biointerface Res Appl Chem* **2021**, *11*, 14555–14563, https://doi.org/10.33263/BRIAC116.1455514563.
13. Reddy Jedla, M.; Koneru, B.; Franco Jr, A.; Rangappa, D.; Banerjee, P. Recent Developments in Nanomaterials Based Adsorbents for Water Purification Techniques. *Biointerface Res Appl Chem* **2021**, *12*, 5821–5835, https://doi.org/10.33263/BRIAC125.58215835.
14. Sengupta, S.; Pari, A.; Biswas, L.; Shit, P.; Bhattacharyya, K.; P. Chattopadhyay, A. Adsorption of Arsenic on Graphene Oxide, Reduced Graphene Oxide, and Their Fe3O4 Doped Nanocomposites. *Biointerface Res Appl Chem* **2021**, *12*, 6196–6210, https://doi.org/10.33263/BRIAC125.61966210.
15. Dutta, S.; Gupta, B.; Srivastava, S.K.; Gupta, A.K. Recent Advances on the Removal of Dyes from Wastewater Using Various Adsorbents: A Critical Review. *Mater. Adv.* **2021**, *2*, 4497–4531, https://doi.org/10.1039/D1MA00354B.
16. Vimonses, V.; Lei, S.; Jin, B.; Chow, C.W.K.; Saint, C. Kinetic Study and Equilibrium Isotherm Analysis of Congo Red Adsorption by Clay Materials. *Chemical Engineering Journal* **2009**, *148*, 354–364, https://doi.org/10.1016/j.cej.2008.09.009.
17. Karaoğlu, M.H.; Doğan, M.; Alkan, M. Kinetic Analysis of Reactive Blue 221 Adsorption on Kaolinite. *Desalination* **2010**, *256*, 154–165, https://doi.org/10.1016/j.desal.2010.01.021.
18. Ray, S.; Kalamdhad, A.S.; Mishra, A.K. Bentonites as a Copper Adsorbent: Equilibrium, PH, Agitation, Dose, and Kinetic Effect Studies. *J. Hazard. Toxic Radioact. Waste* **2020**, *24*, 04019027, https://doi.org/10.1061/(ASCE)HZ.2153-5515.0000476.
19. Amrhar, O.; Nassali, H.; S. Elyoubi, M. Adsorption of a Cationic Dye, Methylene Blue, OntoMoroccan Illitic Clay. *J. Mater. Environ. Sci.* **2015**, 3054–3065, https://www.jmaterenvironsci.com/Document/vol6/vol6_N11/356-JMES-1645-2015-Amrhar.pdf.
20. Borisover, M.; Davis, J.A. Adsorption of Inorganic and Organic Solutes by Clay Minerals. In *Developments in Clay Science*; Elsevier, **2015**, *6*, 33–70, https://doi.org/10.1016/B978-0-08-100027-4.00002-4.
21. Tazi, S.; Rotenberg, B.; Salanne, M.; Sprik, M.; Sulpizi, M. Absolute Acidity of Clay Edge Sites from Ab-Initio Simulations. *Geochimica et Cosmochimica Acta* **2012**, *94*, 1–11, https://doi.org/10.1016/j.gca.2012.07.010.
22. Missana, T.; Alonso, U.; García-Gutiérrez, M. Experimental Study and Modelling of Selenite Sorption onto Illite and Smectite Clays. *Journal of Colloid and Interface Science* **2009**, *334*, 132–138, https://doi.org/10.1016/j.jcis.2009.02.059.
23. Narayanaswamy, V.; Alaabed, S.; AL-Akhras, M.-A.; Obaidat, I.M. Molecular Simulation of Adsorption of Methylene Blue and Rhodamine B on Graphene and Graphene Oxide for Water Purification. *Materials Today: Proceedings* **2020**, *28*, 1078–1083, https://doi.org/10.1016/j.matpr.2020.01.086.
24. Sharma, S. *Molecular Dynamics Simulation of Nanocomposites Using BIOVIA Materials Studio, Lammps and Gromacs*; Elsevier, **2019**, https://www.sciencedirect.com/book/9780128169544/molecular-dynamics-simulation-of-nanocomposites-using-biovia-materials-studio-lammps-and-gromacs.
25. Regti, A.; Lakbaibi, Z.; ben elayouchia, H.; El Haddad, M.; Laamari, M.R.; Jaafar, A.; Elazhary, I.; El Himri, M. Optimization and Computational Approach to Understand the Adsorption Behavior of Alizarine Red S on the Surface of Fish Scales. *Biointerface Res Appl Chem* **2021**, *11*, 14918–14934, https://doi.org/10.33263/BRIAC116.1491814934.
26. Greathouse, J.A.; Geatches, D. l.; Pike, D.Q.; Greenwell, H.C.; Johnston, C.T.; Wilcox, J.; Cygan, R.T. Methylene Blue Adsorption on the Basal Surfaces of Kaolinite: Structure and Thermodynamics from Quantum and Classical Molecular Simulation. *Clays Clay Miner.* **2015**, *63*, 185–198, https://doi.org/10.1346/CCMN.2015.0630303.
27. El Haouti, R.; Ouachtak, H.; El Guerdaoui, A.; Amedlous, A.; Amaterz, E.; Haounati, R.; Addi, A.A.; Akbal, F.; El Alem, N.; Taha, M.L. Cationic Dyes Adsorption by Na-Montmorillonite Nano Clay: Experimental Study Combined with a Theoretical Investigation Using DFT-Based Descriptors and Molecular Dynamics Simulations. *Journal of Molecular Liquids* **2019**, *290*, 111139, https://doi.org/10.1016/j.molliq.2019.111139.

28. Lammers, L.N.; Bourg, I.C.; Okumura, M.; Kolluri, K.; Sposito, G.; Machida, M. Molecular Dynamics Simulations of Cesium Adsorption on Illite Nanoparticles. *Journal of Colloid and Interface Science* **2017**, *490*, 608–620, https://doi.org/10.1016/j.jcis.2016.11.084.
29. Qiu, S.; Qiu, T.; Yan, H.; Long, Q.; Wu, H.; Li, X.; Zhu, D. Investigation of Protonation and Deprotonation Processes of Kaolinite and Its Effect on the Adsorption Stability of Rare Earth Elements. *Colloids and Surfaces A: Physicochemical and Engineering Aspects* **2022**, *642*, 128596, https://doi.org/10.1016/j.colsurfa.2022.128596.
30. Abbou, B.; Lebkiri, I.; Ouaddari, H.; Kadiri, L.; Ouass, A.; Habsaoui, A.; Lebkiri, A.; Rifi, E.H. Removal of Cd(II), Cu(II), and Pb(II) by Adsorption onto Natural Clay: A Kinetic and Thermodynamic Study. *Turk J Chem* **2021**, *45*, 362–376, https://doi.org/10.3906/kim-2004-82.
31. Es-sahbany, H.; Hsissou, R.; El Hachimi, M.L.; Allaoui, M.; Nkhili, S.; Elyoubi, M.S. Investigation of the Adsorption of Heavy Metals (Cu, Co, Ni and Pb) in Treatment Synthetic Wastewater Using Natural Clay as a Potential Adsorbent (Sale-Morocco). *Materials Today: Proceedings* **2021**, *45*, 7290–7298, https://doi.org/10.1016/j.matpr.2020.12.1100.
32. Turan, N.G.; Elevli, S.; Mesci, B. Adsorption of Copper and Zinc Ions on Illite: Determination of the Optimal Conditions by the Statistical Design of Experiments. *Applied Clay Science* **2011**, *52*, 392–399, https://doi.org/10.1016/j.clay.2011.04.010.
33. Gu, S.; Kang, X.; Wang, L.; Lichtfouse, E.; Wang, C. Clay Mineral Adsorbents for Heavy Metal Removal from Wastewater: A Review. *Environ Chem Lett* **2019**, *17*, 629–654, https://doi.org/10.1007/s10311-018-0813-9.
34. Baize, D. *Guide des analyses en pédologie: 2e édition, revue et augmentée*; Editions Quae, 2000; ISBN 978-2-7380-0892-3, https://books.google.ro/books/about/Guide_des_analyses_en_p%C3%A9dologie.html?id=6dL3RK0m_MQC&redir_esc=y.
35. Carroll, D. ION EXCHANGE IN CLAYS AND OTHER MINERALS. *Geol Soc America Bull* **1959**, *70*, 749, https://doi.org/10.1130/0016-7606(1959)70[749:IEICAO]2.0.CO;2.
36. Choy, J.-H.; Park, M. Cationic and Anionic Clays for Biological Applications. In *Interface Science and Technology*; Elsevier, **2004**, *1*, 403–424, http://dx.doi.org/10.1016/S1573-4285(04)80049-8.
37. Liu, Y.; Alessi, D.S.; Flynn, S.L.; Alam, Md.S.; Hao, W.; Gingras, M.; Zhao, H.; Konhauser, K.O. Acid-Base Properties of Kaolinite, Montmorillonite and Illite at Marine Ionic Strength. *Chemical Geology* **2018**, *483*, 191–200, https://doi.org/10.1016/j.chemgeo.2018.01.018.
38. Santamarina, J.C.; Klein, K.A.; Wang, Y.H.; Prencke, E. Specific Surface: Determination and Relevance. *Can. Geotech. J.* **2002**, *39*, 233–241, https://doi.org/10.1139/t01-077.
39. Giles, C.H.; Smith, D.; Huitson, A. A General Treatment and Classification of the Solute Adsorption Isotherm. I. Theoretical. *Journal of Colloid and Interface Science* **1974**, *47*, 755–765, https://doi.org/10.1016/0021-9797(74)90252-5.
40. Limousin, G.; Gaudet, J.-P.; Charlet, L.; Szenknect, S.; Barthès, V.; Krimissa, M. Sorption Isotherms: A Review on Physical Bases, Modeling and Measurement. *Applied Geochemistry* **2007**, *22*, 249–275, https://doi.org/10.1016/j.apgeochem.2006.09.010.
41. Errais, E. Réactivité de Surface d'argiles Naturelles : Etude de l'adsorption de Colorants Anioniques, Strasbourg, **2011**, https://publication-theses.unistra.fr/public/theses_doctorat/2011/ERRAIS_Emna_2011.pdf.
42. Weber, W.J.; Smith, E.H. Activated Carbon Adsorption: The State of the Art. In *Studies in Environmental Science*; Elsevier, **1986**; *29*, pp. 455–492, https://doi.org/10.1016/S0166-1116(08)70958-0.
43. Sarkar, M.; Acharya, P.K.; Bhattacharya, B. Modeling the Adsorption Kinetics of Some Priority Organic Pollutants in Water from Diffusion and Activation Energy Parameters. *Journal of Colloid and Interface Science* **2003**, *266*, 28–32, https://doi.org/10.1016/S0021-9797(03)00551-4.
44. Malash, G.F.; El-Khaiary, M.I. Piecewise Linear Regression: A Statistical Method for the Analysis of Experimental Adsorption Data by the Intraparticle-Diffusion Models. *Chemical Engineering Journal* **2010**, *163*, 256–263, https://doi.org/10.1016/j.cej.2010.07.059.
45. Freundlich, H.M.F. Uber Die Adsorption in Lasungen. *Journal of Physical Chemistry* **1909**, *57*, 385–370, https://doi.org/10.1515/zpch-1907-5723.
46. Langmuir, I. The Adsorption of Gases on Plane Surfaces of Glass, Mica and Platinum. *J. Am. Chem. Soc* **1918**, *40*, 1361-1403, https://doi.org/10.1021/ja02242a004.

47. Dubinin, M.M. The Potential Theory of Adsorption of Gases and Vapors for Adsorbents with Energetically Nonuniform Surfaces. *Chem. Rev.* **1960**, *60*, 235-241, https://doi.org/10.1021/cr60204a006.
48. Temkin, M.; Pyzhev, V. Kinetics of the Synthesis of Ammonia on Promoted Iron Catalysts. *Jour. Phys. Chem. (U.S.S.R.)* **1939**, *13*, 851–867, https://www.scirp.org/(S(351jmbntvnsjt1aadkposzje))/reference/ReferencesPapers.aspx?ReferenceID=128945.
49. Mobarak, M.; Mohamed, E.A.; Selim, A.Q.; Mohamed, F.M.; Sellaoui, L.; Bonilla-Petriciolet, A.; Seliem, M.K. Statistical Physics Modeling and Interpretation of Methyl Orange Adsorption on High–Order Mesoporous Composite of MCM–48 Silica with Treated Rice Husk. *Journal of Molecular Liquids* **2019**, *285*, 678–687, https://doi.org/10.1016/j.molliq.2019.04.116.
50. Selim, A.Q.; Sellaoui, L.; Mobarak, M. Statistical Physics Modeling of Phosphate Adsorption onto Chemically Modified Carbonaceous Clay. *Journal of Molecular Liquids* **2019**, *279*, 94–107, https://doi.org/10.1016/j.molliq.2019.01.100.
51. Amrhar, O.; El Gana, L.; Mobarak, M. Calculation of Adsorption Isotherms by Statistical Physics Models: A Review. *Environ Chem Lett* **2021**, https://doi.org/10.1007/s10311-021-01279-8.
52. Furusawa, T.; Smith, J.M. Fluid-Particle and Intraparticle Mass Transport Rates in Slurries. *Industrial & Engineering Chemistry Fundamentals* **1973**, *12*, 197–203, https://doi.org/10.1021/i160046a009.
53. Boyd, G.E.; Adamson, A.W.; Myers, L.S. The Exchange Adsorption of Ions from Aqueous Solutions by Organic Zeolites. II. Kinetics. *Journal of the American Chemical Society* **1947**, *69*, 2836–2848, https://doi.org/10.1021/ja01203a066.
54. Weber, W.J.; Morris, J.C. Kinetics of Adsorption Carbon from Solutions. *Journal Sanitary Engeering Division Proceedings.American Society of Civil Engineers* **1963**, *89*, 31–60, https://ascelibrary.org/doi/abs/10.1061/JSEDAI.0000430.
55. Lagergren, S. Zur Theorie Der Sogenannten Adsorption Geloster Stoffe. *Kungliga Svenska Vetenskapsakademiens, Handlingar* **1898**, *24*, 1–39, https://link.springer.com/article/10.1007/BF01501332.
56. Blanchard, G.; Maunaye, M.; Martin, G. Removal of Heavy Metals from Waters by Means of Natural Zeolites. *Water Research* **1984**, *18*, 1501–1507, https://doi.org/10.1016/0043-1354(84)90124-6.
57. Ho, Y. Review of Second-Order Models for Adsorption Systems. *Journal of Hazardous Materials* **2006**, *136*, 681–689, https://doi.org/10.1016/j.jhazmat.2005.12.043.
58. Drits, V.A.; Zviagina, B.B.; McCarty, D.K.; Salyn, A.L. Factors Responsible for Crystal-Chemical Variations in the Solid Solutions from Illite to Aluminoceladonite and from Glauconite to Celadonite. *American Mineralogist* **2010**, *95*, 348–361, https://doi.org/10.2138/am.2010.3300.
59. Material Studio Modeling DS Biovia - Dassault Systemes, San Diego 2016.
60. Galván-García, E.A.; Agacino-Valdés, E.; Franco-Pérez, M.; Gómez-Balderas, R. [Cu(H2O) n]2+ (n = 1–6) Complexes in Solution Phase: A DFT Hierarchical Study. *Theor Chem Acc* **2017**, *136*, 29, https://doi.org/10.1007/s00214-017-2056-4.
61. Burda, J.V.; Pavelka, M.; Šimánek, M. Theoretical Model of Copper Cu(I)/Cu(II) Hydration. DFT and Ab Initio Quantum Chemical Study. *Journal of Molecular Structure: THEOCHEM* **2004**, *683*, 183–193, https://doi.org/10.1016/j.theochem.2004.06.013.
62. Weston, M.; Reade, T.J.; Handrup, K.; Champness, N.R.; O'Shea, J.N. Adsorption of Dipyrrin-Based Dye Complexes on a Rutile TiO_2 (110) Surface. *J. Phys. Chem. C* **2012**, *116*, 18184–18192, https://doi.org/10.1021/jp3025864.
63. Mehmeti, V.; Podvorica, F.I. Experimental and Theoretical Studies on Corrosion Inhibition of Niobium and Tantalum Surfaces by Carboxylated Graphene Oxide. *Materials* **2018**, *11*, 893, https://doi.org/10.3390/ma11060893.
64. Sun, H. COMPASS: An Ab Initio Force-Field Optimized for Condensed-Phase ApplicationsOverview with Details on Alkane and Benzene Compounds. *J. Phys. Chem. B* **1998**, *102*, 7338–7364, https://doi.org/10.1021/jp980939v.
65. Sun, H.; Ren, P.; Fried, J.R. The COMPASS Force Field: Parameterization and Validation for Phosphazenes. *Computational and Theoretical Polymer Science* **1998**, *8*, 229–246, https://doi.org/10.1016/S1089-3156(98)00042-7.
66. Xu, Y.; Liu, Y.-L.; Liu, G.-S. Molecular Dynamics Simulation of Primary Ammonium Ions with Different Alkyl Chains on the Muscovite (001) Surface. *International Journal of Mineral Processing* **2015**, *145*, 48–56, https://doi.org/10.1016/j.minpro.2015.07.003.

67. Berisha, A.; Podvoricaa, F.I. The Adsorption of Aryldiazonium Salts onto the (8,8) Single-Wall Carbon Nanotubes -an "Ab Initio" and Monte Carlo Study. *Research* **2019**, *24*, https://www.researchgate.net/publication/337946811_The_adsorption_of_aryldiazonium_salts_onto_the_88_Single-Wall_Carbon_Nanotubes_-an_Ab_initio_and_Monte_Carlo_study.
68. Largo, F.; Haounati, R.; Akhouairi, S.; Ouachtak, H.; El Haouti, R.; El Guerdaoui, A.; Hafid, N.; Santos, D.M.F.; Akbal, F.; Kuleyin, A.; *et al.* Adsorptive Removal of Both Cationic and Anionic Dyes by Using Sepiolite Clay Mineral as Adsorbent: Experimental and Molecular Dynamic Simulation Studies. *Journal of Molecular Liquids* **2020**, *318*, 114247, https://doi.org/10.1016/j.molliq.2020.114247.
69. Chen, Y.; Peng, J.; Xiao, H.; Peng, H.; Bu, L.; Pan, Z.; He, Y.; Chen, F.; Wang, X.; Li, S. Adsorption Behavior of Hydrotalcite-like Modified Bentonite for Pb 2+ , Cu 2+ and Methyl Orange Removal from Water. *Applied Surface Science* **2017**, *420*, 773–781, https://doi.org/10.1016/j.apsusc.2017.05.138.
70. Chu, Y.; Khan, M.A.; Wang, F.; Xia, M.; Lei, W.; Zhu, S. Kinetics and Equilibrium Isotherms of Adsorption of Pb(II) and Cu(II) onto Raw and Arginine-Modified Montmorillonite. *Advanced Powder Technology* **2019**, *30*, 1067–1078, https://doi.org/10.1016/j.apt.2019.03.002.
71. Bourliva, A.; Sikalidis, A.K.; Papadopoulou, L.; Betsiou, M.; Michailidis, K.; Sikalidis, C.; Filippidis, A. Removal of Cu2+ and Ni2+ Ions from Aqueous Solutions by Adsorption onto Natural Palygorskite and Vermiculite. *Clay Minerals* **2018**, *53*, 1–15, https://doi.org/10.1180/clm.2017.1.
72. Bradl, H.B. Adsorption of Heavy Metal Ions on Soils and Soils Constituents. *Journal of Colloid and Interface Science* **2004**, *277*, 1–18, https://doi.org/10.1016/j.jcis.2004.04.005.
73. Bellir, K.; Bouziane, I.S.; Boutamine, Z.; Lehocine, M.B.; Meniai, A.-H. Sorption Study of a Basic Dye "Gentian Violet" from Aqueous Solutions Using Activated Bentonite. *Energy Procedia* **2012**, *18*, 924–933, https://doi.org/10.1016/j.egypro.2012.05.107.
74. Sdiri, A.T.; Higashi, T.; Jamoussi, F. Adsorption of Copper and Zinc onto Natural Clay in Single and Binary Systems. *International Journal of Environmental Science and Technology* **2014**, *11*, 1081–1092, https://doi.org/10.1007/s13762-013-0305-1.
75. Mozaffari Majd, M.; Kordzadeh-Kermani, V.; Ghalandari, V.; Askari, A.; Sillanpää, M. Adsorption Isotherm Models: A Comprehensive and Systematic Review (2010−2020). *Science of The Total Environment* **2022**, *812*, 151334, https://doi.org/10.1016/j.scitotenv.2021.151334.
76. Helfferich, F. *Ion Exchange*; McGraw-Hill, New York, **1962**; ISBN 0-486-68784-8, https://www.science.org/doi/10.1126/science.138.3537.133.a.
77. Atrous, M.; Sellaoui, L.; Bouzid, M.; Lima, E.C.; Thue, P.S.; Bonilla-Petriciolet, A.; Ben Lamine, A. Adsorption of Dyes Acid Red 1 and Acid Green 25 on Grafted Clay: Modeling and Statistical Physics Interpretation. *Journal of Molecular Liquids* **2019**, *294*, 111610, https://doi.org/10.1016/j.molliq.2019.111610.
78. Nakhli, A.; Khalfaoui, M.; Aguir, C.; Bergaoui, M.; M'henni, M.F.; Ben Lamine, A. Statistical Physics Studies of Multilayer Adsorption on Solid Surface: Adsorption of Basic Blue 41 Dye onto Functionalized *Posidonia* Biomass. *Separation Science and Technology* **2014**, *49*, 2525–2533, https://doi.org/10.1080/01496395.2014.929703.
79. Sellaoui, L.; Dotto, G.L.; Lamine, A.B.; Erto, A. Interpretation of Single and Competitive Adsorption of Cadmium and Zinc on Activated Carbon Using Monolayer and Exclusive Extended Monolayer Models. *Environ Sci Pollut Res* **2017**, *24*, 19902–19908, https://doi.org/10.1007/s11356-017-9562-8.
80. Dotto, G.L.; Sellaoui, L.; Lima, E.C.; Lamine, A.B. Physicochemical and Thermodynamic Investigation of Ni(II) Biosorption on Various Materials Using the Statistical Physics Modeling. *Journal of Molecular Liquids* **2016**, *220*, 129–135, https://doi.org/10.1016/j.molliq.2016.04.075.
81. Wjihi, S.; Peres, E.C.; Dotto, G.L.; Lamine, A.B. Physicochemical Assessment of Crystal Violet Adsorption on Nanosilica through the Infinity Multilayer Model and Sites Energy Distribution. *Journal of Molecular Liquids* **2019**, *280*, 58–63, https://doi.org/10.1016/j.molliq.2018.12.064.
82. Sellaoui, L.; Guedidi, H.; SarraWjihi, S.; Reinert, L.; Knani, S.; Duclaux, L.; Ben Lamine, A. Experimental and Theoretical Studies of Adsorption of Ibuprofen on Raw and Two Chemically Modified Activated Carbons: New Physicochemical Interpretations. *RSC Adv.* **2016**, *6*, 12363–12373, https://doi.org/10.1039/C5RA22302D.
83. Ayachi, F.; Z. Kyzas, G.; Aatrous, M.; Sakly, A.; Ben Lamine, A. Evaluating the Adsorption of Ni(II) and Cu(II) on Spirulina Biomass by Statistical Physics Formalism. *Journal of Industrial and Engineering Chemistry* **2019**, *80*, 461–470, https://doi.org/10.1016/j.jiec.2019.05.044.

84. Sheikhhosseini, A.; Shirvani, M.; Shariatmadari, H. Competitive Sorption of Nickel, Cadmium, Zinc and Copper on Palygorskite and Sepiolite Silicate Clay Minerals. *Geoderma* **2013**, *192*, 249–253, https://doi.org/10.1016/j.geoderma.2012.07.013.
85. Shahmohammadi-Kalalagh, S.; Babazadeh, H.; Nazemi, A.H.; Manshouri, M. Isotherm and Kinetic Studies on Adsorption of Pb, Zn and Cu by Kaolinite. *Caspian Journal of Environmental Sciences* **2011**, *9*, 243–255, https://www.researchgate.net/publication/266874259_Isotherm_and_Kinetic_Studies_on_Adsorption_of_Pb_Zn_and_Cu_by_Kaolinite.
86. Ijagbemi, C.O.; Baek, M.-H.; Kim, D.-S. Montmorillonite Surface Properties and Sorption Characteristics for Heavy Metal Removal from Aqueous Solutions. *Journal of Hazardous Materials* **2009**, *166*, 538–546, https://doi.org/10.1016/j.jhazmat.2008.11.085.
87. Doula, M.K.; Dimirkou, A. Use of an Iron-Overexchanged Clinoptilolite for the Removal of Cu2+ Ions from Heavily Contaminated Drinking Water Samples. *Journal of Hazardous Materials* **2008**, *151*, 738–745, https://doi.org/10.1016/j.jhazmat.2007.06.047.
88. Mohapatra, M.; Mohapatra, L.; Singh, P.; Anand, S.; Mishra, B.K. A Comparative Study on Pb(II), Cd(II), Cu(II), Co(II) Adsorption from Single and Binary Aqueous Solutions on Additive Assisted Nano-Structured Goethite. *International Journal of Engineering, Science and Technology* **2010**, *2*, 89–103, http://dx.doi.org/10.4314/ijest.v2i8.63784.
89. Salhi, A.; Tighadouini, S.; El-Massaoudi, M.; Elbelghiti, M.; Bouyanzer, A.; Radi, S.; El Barkany, S.; Bentiss, F.; Zarrouk, A. Keto-Enol Heterocycles as New Compounds of Corrosion Inhibitors for Carbon Steel in 1 M HCl: Weight Loss, Electrochemical and Quantum Chemical Investigation. *Journal of Molecular Liquids* **2017**, *248*, 340–349, https://doi.org/10.1016/j.molliq.2017.10.040.

Supplementary Information

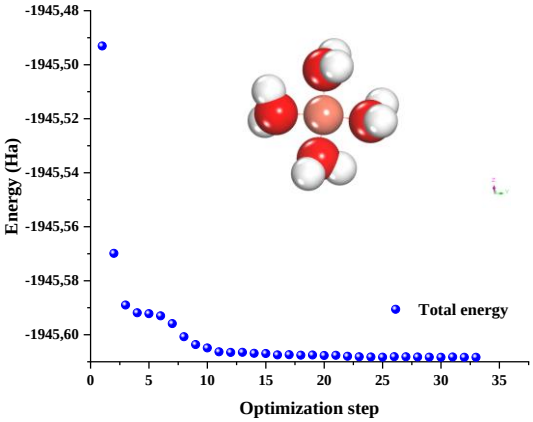

Figure S1. Geometry optimization of $Cu[(H_2O)_4]^{2+}$ using $Dmol^3$ module according to GGA/PBE functional. Atoms of Cu, O, and H are reddish, red, and white, respectively.

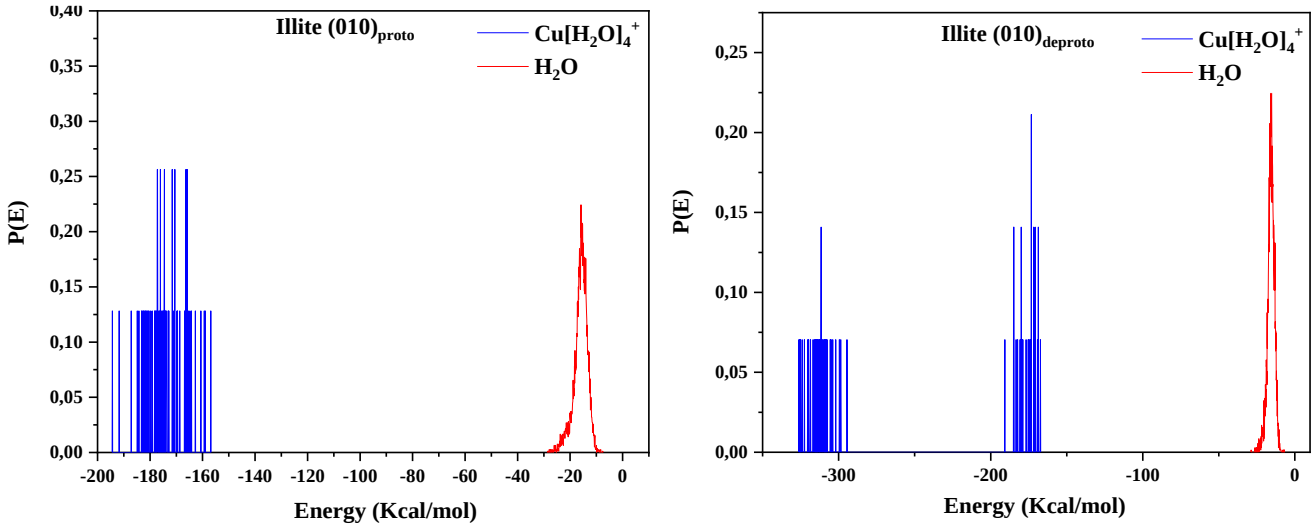

Figure S2. Adsorption energy distribution of $[Cu(H_2O)_4]^{2+}$ onto illite $(010)_{proto}$ and illite $(010)_{deproto}$ surfaces.

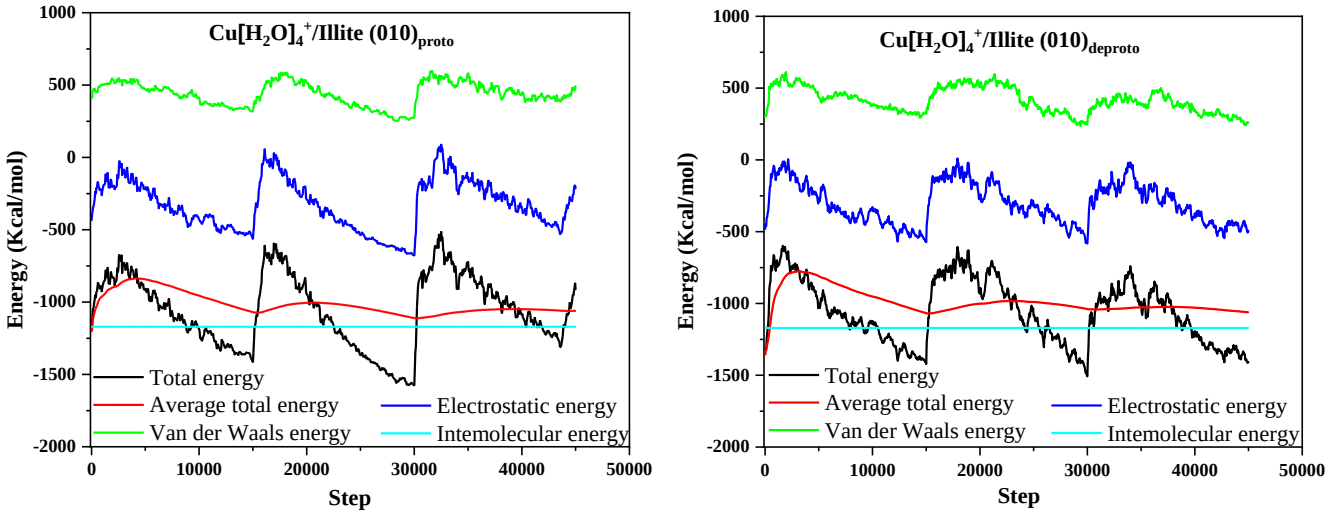

Figure S3. Fluctuations of interaction energies corresponding to $[Cu(H_2O)_4]^{2+}$/illite $(010)_{proto}$ and $[Cu(H_2O)_4]^{2+}$/illite $(010)_{deproto}$ systems.